Deformable Organisms and Error Learning for Brain Segmentation

Gautam Prasad[1,2], Anand A. Joshi[3],
Albert Feng[1], Marina Barysheva[1] Katie L. McMahon[4],
Greig I. de Zubicaray[5], Nicholas G. Martin[4], Margaret J. Wright[4],
Arthur W. Toga[1], Demetri Terzopoulos[2], and Paul M. Thompson[1]

[1]Laboratory of Neuro Imaging, Department of Neurology, UCLA School of Medicine, Los Angeles, CA, USA
[2]Department of Computer Science, UCLA, Los Angeles, CA, USA
[3]Signal and Image Processing Institute, University of Southern California, Los Angeles, CA, USA
[4]Queensland Institute of Medical Research, Brisbane, Australia
[5]School of Psychology, University of Queensland, Brisbane, Australia

Abstract. Segmentation methods for medical images may not generalize well to different data sets or tasks, hampering their utility. We attempt to remedy these issues using deformable organisms to create an easily customizable segmentation plan. This plan is developed by borrowing ideas from artificial life to govern a set of deformable models that use control processes such as sensing, proactive planning, reactive behavior, and knowledge representation to segment an image. The image may have landmarks and features specific to that dataset; these may be easily incorporated into the plan. We validate this framework by creating a plan to locate the brain in 3D magnetic resonance images of the head (skull-stripping). This is important for surgical planning, understanding how diseases affect the brain, conducting longitudinal studies, registering brain data, and creating cortical surface models. Our plan dictates how deformable organisms find features in head images and cooperatively work to segment the brain. In addition, we use a method based on Adaboost to learn and correct errors in our segmentation. We tested our method on 630 T1-weighted images from healthy young adults, evaluating results using distance and overlap error metrics based on expert gold standard segmentations. We compare our segmentations with and without the error correction step; we also compare our results to three other widely used methods: BSE, BET, and the Hybrid Watershed algorithm. Our method had the least Hausdorff distance to expert segmentations on this dataset, but included slightly more non-brain voxels (false positives). Our framework captures diverse categories of information needed for skull-stripping, and produces competitive segmentations.

Keywords: deformable organisms, segmentation, MRI, Adaboost, Hausdorff, overlap, registration

1 Introduction

Deformable organisms label objects in images by integrating high level control mechanisms into a segmentation plan. They combine sensing, knowledge representation, reactive behavior, and proactive planning so our devised organisms may cooperatively segment an image. Deformable organisms were introduced into medical imaging by [13] who combined ideas from artificial life [29] and deformable models [14, 30]. Since their introduction, deformable organisms have been used for limb delineation [18], and segmentation of the spinal cord [16], vasculature [17], and corpus callosum in the brain [6]. [15] created a deformable organisms framework using the Insight Toolkit (ITK) [8], but we did not use it here, as its capabilities were too basic for our application. In contrast to several brain segmentation methods that work with low-level image processing and computer vision techniques, our deformable organisms can incorporate high-level knowledge and expectations regarding image data. In addition, almost every step of the plan presented here differs significantly from the one we previously presented [21].

Segmenting brain from non-brain tissues (such as the eyes, skull, scalp, and neck) in magnetic resonance (MR) images of the head is a vital pre-processing step for many types of image analysis. Accurate masks of the brain are helpful for longitudinal studies [22], for multi-subject analyses of brain structure and function [31], and as a pre-processing step prior to cortical surface modeling [32], surgical planning [4], and brain registration [34].

The process of segmenting brain versus non-brain tissue on MRI is commonly referred to as "skull-stripping" (although, strictly speaking, the skull generates almost no signal on T1-weighted MRI and the scalp and meninges are the main tissues removed). This has traditionally been done manually by trained experts, or by automated methods that are subsequently corrected by hand. Manually-created masks may also be used as gold standard delineations to validate performance of skull-stripping methods based on different principles. Though many approaches have been developed for this task, time consuming manual clean-up of these generated masks is almost always required. Most published methods do not perform well on all datasets, making improvements over existing methods critical.

There are a variety of existing skull-stripping methods. The Brain Extraction Tool (BET) [28] evolves a deformable model to find the boundary of the brain. It provides a robust way to find the boundary in unclear regions but does not incorporate prior knowledge of the brain's shape. The Brain Surface Extractor (BSE) [25] uses edge detection and morphological operations to find the brain/non-brain boundary. BSE quickly extracts the brain from an image but may include extra material in the mask, as it sometimes fails to remove connections between the brain and surrounding tissue. The Hybrid Watershed Algorithm (HWA) [24] uses the watershed algorithm to find the brain region, then fits a deformable model to the region, and finally deforms it based on a statistical atlas and geometric constraints. These methods have also been analyzed

in [1]. We chose these methods as they are the most widely used and are part of larger neuroimaging toolkits.

We create a deformable organism plan that governs a collection of organisms to segment different parts of the head and brain. The organisms evolve dynamically in the images and cooperatively compute an accurate and robust segmentation of the brain. We then use a learning method, based on an Adaboost wrapper, [33], to classify the error in our method. We evaluate the effectiveness of this additional error correction step in improving our segmentations. We test our method with 630 T1-weighted MR images from healthy young adults, aged 20-30 years. We compare our approach to three widely used methods and we validate our results using distance, overlap, and error metrics.

2 Methods

Our deformable organisms method aims to segment the brain in T1-weighted MR images of the head. We describe our deformable organism plan to segment the brain, a way to learn and correct errors in our method, validation metrics to compare our results to the gold standard and to other widely-used methods, and our experimental results.

2.1 Deformable Organisms

Deformable organisms are organized in five different layers that combine control mechanisms and different representations to segment an image. We adapt this general approach for segmenting the brain.

Geometry and Physics We represent each organism as a 3D triangulated mesh. These meshes are initialized on a standard brain template image. Our template was selected from the 40 images in the LONI Probabilistic Brain Atlas (LPBA40) [26], which have corresponding manual segmentations for 56 structures, and have manual delineations of the brain boundary. In the image we selected from this set, the voxels lying in each of our regions of interest are labeled. We fit our organisms to these labels to create a mesh using a marching cubes method [12] that goes through the image. The mesh is made up of polygons representing the border of the regions, which are then fused together.

These meshes deform to fit the 3D region that their corresponding organism is modeling. This iterative process moves each of the mesh's vertices along its normal direction with respect to the mesh surface. The surface is smoothed at every iteration using curvature weighted smoothing [2, 19]. This smoothing technique attenuates noise through a diffusion process as

$$\frac{\partial \mathbf{S}}{\partial t} = \lambda L(\mathbf{S}), \tag{1}$$

where S is the mesh, surface, or manifold and L is the Laplacian, which is equivalent to the total curvature of the surface. This Laplacian is linearly approximated by

$$L(\mathbf{v}_i) = w_{ji} \sum \mathbf{v}_j - \mathbf{v}_{i_{j \in N(i)}}, \tag{2}$$

where v_i is the vertex i in the mesh, $N(i)$ are the neighbors of i, and w_{ji} is a weight proportional to the curvature between vertices j and i. We smooth the

mesh to constrain its deformations to prevent intersections and artifacts from corrupting the boundary. On the boundary, we sample from the surrounding image.

Our prior based on an image from LPBA40 precludes us from using the Segmentation Validation Engine tool [27] to validate our method as it would lead to an unfair bias that would be favorable to our method; instead we use other metrics (below).

Perception Our organisms "sense" the encompassing image by sampling its intensities at vertices of the mesh. The vertices composing the mesh have real-valued coordinates, so we used nearest neighbor interpolation to find the intensities that correspond to them in the discrete grid of voxels in the image. The images may be any of the subject-derived volumes, which include the threshold image, 2-means classified image, 3-means classified image, or gradient image.

Paramount to the perception layer is the organisms' ability to sense each other's locations. We locate the voxels an organism resides on using a 3D rasterization algorithm [20, 5] that efficiently computes these values. These locations allow our organisms to dynamically change the way they deform based on their own positions and intensities of the original T1-weighted subject image.

Motor Control We move the vertices of the mesh along their normal direction with respect to the mesh surface by analyzing a set of intensities along this normal line. We describe the evolution of our mesh or surface $S(i,t)$ with respect to time t, where i is a vertex or point on the surface, as

$$\frac{\partial \mathbf{S}(i,t)}{\partial t} = F(\mathbf{P}, \mathbf{n}, \mathbf{I}_d, b(c,l)_j)\mathbf{n}, \tag{3}$$

with F being the speed of evolution. F samples a set of positions P along point i's normal and interpolates these values from any of the derived images I_d, where d specifies the set of derived image. That set consists of the threshold image (t), 2-means image (2), 3-means image (3), and gradient image (g). The function $b(c)_j$ specifies any of a number of behaviors and decides how to move the point i on the surface by analyzing the sampled intensities l subject to a set of constraints, and weights the movement by the scalar c.

In practice, we evolve each vertex by the amount specified by F along its normal and progress through time by iterating through all vertices in the mesh until there is no longer any significant movement.

Behavior Our behaviors are a higher level of abstraction to indicate how the organisms function and what information they need to find. Behaviors may prescribe a function for organisms to be attracted to or repelled from landmarks or help converge on the boundary of an object. The functions for our behaviors had specific tasks in mind in the context of skull-stripping but are general and simple enough for repeated use in any segmentation task.

We developed six behaviors that play an important role in almost every step of our skull-stripping plan.

1. We create a behavior that analyzes a binary image and locates a boundary in these images. It contracts if a vertex corresponds to an off value and expands if it corresponds to an on value, and may be described as

$$b(c,l)_1 = \begin{cases} -c & \text{if } l_i = 0 \\ c & \text{otherwise} \end{cases} \tag{4}$$

   In this case the set l consists of a single value l_i, the value of the binary image that corresponds to the vertex i.
2. Our second behavior moves a vertex outwards if its corresponding intensity value is q and may be described as

$$b(c,l)_2 = \begin{cases} c & \text{if } l_i = q \\ 0 & \text{otherwise} \end{cases} \tag{5}$$

   Its purpose is to expand into an area of an image with voxels having intensities q. In addition q may be a set of labels that are appropriate for expansion.
3. Our third behavior is customized to move our skin mesh through the skull and skin into the cerebrospinal fluid (CSF). It contracts itself further if the boundary intersects another organism (in our plan, the other organisms are the eyes and we wish to deform through those areas) and will check the intensities (l) along the normal for those that correspond to CSF. If CSF markers m are found (signified by very low intensity values and a specific label in our k-means images) we contract the mesh, and if they are deficient, we expand the mesh. This behavior may be represented as

$$b(c,l)_3 = \begin{cases} -c & \text{if } l_i \text{ intersects other organism} \\ -c & \text{if } m \in l \\ c & \text{if } m \notin l \\ 0 & \text{otherwise} \end{cases} \tag{6}$$

   In our framework, the intensities, l, are sampled from the k-means images and m is the label corresponding to CSF. The sampled points are locations inside the surface with respect to i.
4. the fourth behavior we created was designed for the brain organism to locate the boundary of the brain. It contracts vertices away from other organisms, contracts if there are CSF marker values (m) present within the surface, expands if the label value at i is not q, and expands if the gradient intensity at l_i is greater than or equal to a threshold t. The precedence of these constraints is ordered as

$$b(c,l)_4 = \begin{cases} -c & \text{if } l_i \text{ intersects other organism} \\ -c & \text{if } m \in l \\ c & \text{if } l_i \neq q \\ c & \text{if } l_i \leq t \\ 0 & \text{otherwise} \end{cases} \tag{7}$$

   The values at l are sampled from either the 3D rasterization image of the other organisms' meshes, the 3-means classified image, or the gradient image.

5. Our final behavior is the same as behavior 2 but instead of expanding it contracts.

$$b(c,l)_5 = \begin{cases} -c & \text{if } l_i = q \\ 0 & \text{otherwise} \end{cases} \tag{8}$$

Cognition We create a plan of different behaviors to perform a segmentation task. The plan may dynamically activate different behaviors depending on what features the organisms were able to find in the image. Our plan to skull-strip the brain is one such plan.

2.2 Skull-Stripping Plan

Our skull-stripping plan combines our image processing and deformable organisms to create objectives in the image to extract the locations of different regions, culminating in extracting the boundary of the brain. In what follows, we describe each step in detail and how it depends on previous knowledge obtained by organisms. This is just one plan and may be fashioned for any type of segmentation or specifics of the data. Table 1 summarizes the steps each organism takes during the segmentation.

1. We begin by registering the subjects T1-weighted MR image to the template we selected from the LPBA40. This registration step is important to transform subject images into a standard coordinate space as our organisms are tuned (iterations for deformations and labels for k-means classification) to images roughly corresponding to our template. Our template incorporates prior information and may be changed by users who need something closer to their own data. It provides initial locations and shapes for our skin, eye, and brain organisms.
   We used an affine transformation for registration provided by FMRIB's Linear Image Registration Tool (FLIRT) [9]. FLIRT uses the correlation ratio [23] as the metric between the two images that takes the form

$$\frac{1}{Var(Y)} \sum \frac{n_k}{N} Var(Y_k)_k . \tag{9}$$

   Y represents one of the images, $Var(Y)$ is the variance of Y, Y_k is the k-th iso-set i.e. the set of intensities in Y at positions where the other image X has intensities in the kth bin, n_k is the number of values in Y_k with $N = \sum_k n_k$. This cost is optimized to find a 12-parameter affine transformation.
   In addition, we compute the inverse transformation to take the subject image back to its native space at the end of the segmentation.
2. We find the location or boundary of the skin with the skin organism. Its initial shape is of the skin of our template image found using the marching cubes method. We dilated this substantially to ensure we encompass the head of any subject registered to the template. Our template-fitted mesh needs to be further refined to fit our subject. To do this, we analyze the subject's intensities and apply a threshold to create a binary image masking out the head. We also use behavior 1 to sense the threshold image and evolve our

skin organism's mesh to find this perimeter. We iterate the deformations dictated by behavior 1 (applying smoothing at every step) until there is no significant movement of the surface or we reach a maximum iteration bound. We specify this bound based on images being reasonably aligned to the template, an approach we used for all our deformations. The adjacent eyes are handled in a similar manner.

3. Our eye organisms find the eye boundary by sensing the 3-means classified image. We initialize the eye organisms' meshes by fitting them to our template and eroding them to make sure they lie within a subject image's eyeballs. The eyeball locations are found by the organisms sensing the 3-means image with behavior 2, which chooses a label found in the eyeball region.
4. Our next step locates the cerebrospinal fluid (CSF) that surrounds the brain. We achieve this using our skin organism by contracting its mesh into the head through the skin and skull. The skin and skull locations are roughly classified in our 2-means image and we apply behavior 3 to sense it and find the CSF boundary. To further refine this boundary the behavior also makes the skin organism deform through the eye organisms because there is more information about the CSF location by the eyes.
5. This step finds the tissues surrounding the eyeballs that need to be excluded from the brain delineation. We attain this goal by expanding the eye organisms further by sensing the 2-means image along with behavior 2 again, this time behavior 2 looks for a different label in the classified image, one that gives an understanding of tissues around the eyes. The eyes now furnish a better understanding to locate the brain.
6. We complete our plan by finding the brain using our brain organism. Every step in the plan supports of this step and all of our knowledge up to this point will come into play. Our brain organism begins by sensing the 3-means image and gradient image with behavior 4. The behavior is cognizant of the other organisms' locations and uses them to constrain its evolution. With the completion of behavior 4 we further refine the boundary by sensing the 3-means image again with behavior 5, which results in the brain being encapsulated by our brain mesh. The mesh is then converted by the 3D rasterization scheme to a binary volume to which we apply our inverse transform from FLIRT to bring the subject's delineation back into its native space to complete the segmentation.

We make a binary volume of the brain organism and apply the inverse transformation back to the subject image space, completing the segmentation.

3 Error Learning

We are able to learn the types of errors our method makes, by comparing the masks it generated with expert manual delineations. [33] introduced an algorithm using Adaboost [3] to learn a weighting of a set of features used to classify if a voxel has been correctly classified by a prior algorithm. This 'Adaboost wrapper' algorithm uses a set of corresponding automated and manual segmentations, as

Table 1: Plan for each organism to skull-strip an MRI image.

	Skin Organism	Eye Organism	Brain Organism
Initialization		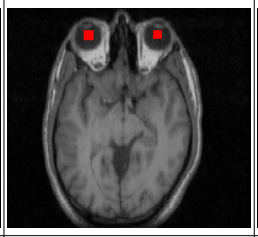	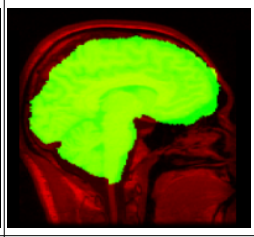
Deformation 1	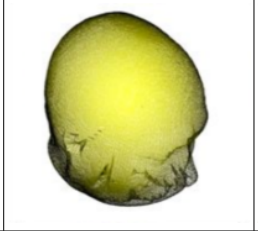	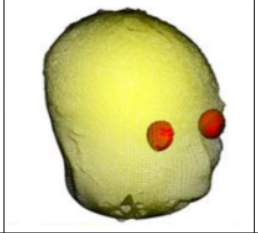	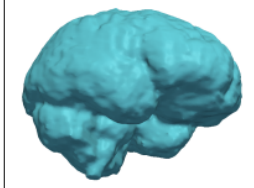
Deformation 2	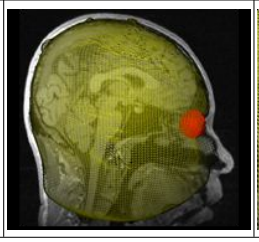	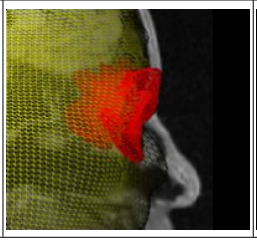	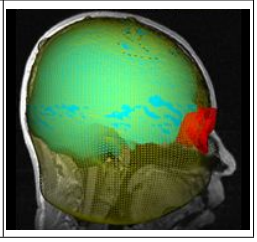

well as intensity images to find features that lie in regions that the first-pass method incorrectly classifies. We use this algorithm to learn situations in which our method makes errors and thereby improve the segmentation.

4 Validation

The masks from the deformable organism method are compared with the gold standard manual segmentations using standard distance, overlap, and error metrics. We use the Hausdorff distance measure [7] to find the distance from the furthest point in the deformable organism method mask to the closest point of the mask in the manual delineation. We also compare the expert and automated masks using the Jaccard coefficient (union overlap), Dice coefficient (mean overlap), false negative rate, and false positive rate described in [11].

We compared the differences in metric values across methods using paired-sample t-tests to understand if their results were statistically different.

5 Experiments

We tested our deformable organism skull stripping method on our set of 630 manually-labeled subject images. In addition, we also ran BET (BET2, FSL 4.1.5, default parameters), BSE (BSE 10a, default parameters), and the Water-

shed algorithm (Freesurfer 5.0.0, default parameters), and assessed their errors using standard distance-based, overlap, and error metrics.

Typically patterns of error in our method were learned by selecting a subset of our segmentation results and using the error learning algorithm (the 'Adaboost wrapper' approach). We then segmented a new subset of images with the error classified and corrected. We repeated this experiment 10 times, using 10 random images from our results to train and 10 random (but non-overlapping) images to test. Masks were then compared to expert ground truth before and after error correction; note that the test set of images was independent of those used for training the error correction step.

6 Results

6.1 Subject Data

Our subject data consisted of 630 T1-weighted magnetic resonance (MR) images from healthy young adults, between 20 and 30 years of age. These images are from Australian twins, and have been used in numerous prior analyses [10].

Each of the images had been manually skull-stripped by a neuroanatomically trained expert. These manual labels were used as the gold standard to compare with automatic segmentation results of our method and the other 3 widely-used methods. The subjects were scanned with a 4-Tesla Bruker Medspec whole-body scanner. 3D T1-weighted images were acquired using a magnetization-prepared rapid gradient echo sequence, resolving the anatomy at high resolution. Acquisition parameters were: inversion time (T_I)/repetition time (T_R)/echo time (T_E)=700/1500/3.35 ms, flip angle=8°, slice thickness=0.9 mm with a $256 \times 256 \times 256$ acquisition matrix.

In addition, we used one of the 40 images from the LONI Probabilistic Brain Atlas (LPBA40) [26]. Each image had 56 different structures manually labeled, including a mask of the brain.

Table 2 shows the distance, overlap, and error metrics for the automated skull-stripping algorithms compared to manual segmentation. We compare BET, BSE, and the Watershed method. Average metrics over the 630 subject images are shown. Our paired-sample t-tests showed the metric values across all the methods were significantly different. These test results showed that the deformable organisms approach was statistically better than the others in the Hausdorff distance and false negative error for our dataset.

The deformable organisms method took a few minutes to run on the subject images we used on a machine with dual 64-bit 2.4 gigahertz AMD Opteron 250 CPU with 8 gigabytes of memory.

We list average results of deformable organisms with and without error correction versus manual training in Table 3. Random samples of 20 images from the 630 were selected, using 10 to train and 10 to test the error correction. We repeat this 10 times and average the results. These average results were used a for two-sample t-test that found statistically significant improvement in Jaccard, Dice, and false positive error metrics.

Table 2: Distance, overlap, and error metrics comparing automated results with manual skull-stripping.

	Hausdorff Distance	Jaccard Overlap	Dice Overlap	False Negative Error	False Positive Error
Deformable Organisms	36.3475±24.3842	0.8478±0.0242	0.9175±0.0143	0.0253±0.0115	0.1328±0.0280
BET	41.7997±24.7972	0.8860±0.0183	0.9395±0.0104	0.0711±0.0218	0.0491±0.0189
BSE	64.7451±25.7714	0.8348±0.1295	0.9040±0.0842	0.1045±0.1456	0.0720±0.0323
Watershed	67.4672±8.7859	0.3650±0.0599	0.5321±0.0617	0.4511±0.0613	0.4831±0.0648

Table 3: Distance, overlap, and error metrics comparing the deformable organisms segmentation with and without error correction versus manual skull-stripping.

	Hausdorff Distance	Jaccard Overlap	Dice Overlap	False Negative Error	False Positive Error
Basic DO	35.4780±2.7890	0.8485±0.0009	0.9178±0.0005	0.0256±0.0006	0.1318±0.0010
DO with correction	35.5194±3.1299	0.8858±0.0013	0.9393±0.0007	0.0253±0.0004	0.0929±0.0012

7 Discussion

The metrics in Table 2 suggest that the performance of our deformable organisms approach is comparable to that of other widely used methods. It has the lowest Hausdorff distance average between its automatic results and the gold standard delineations. It did have a higher false positive error, meaning it may include slightly more voxels inside the boundary of the brain.

Table 3 shows that learning errors improves the segmentation results; all metrics examined were improved, especially the Jaccard coefficient. This additional training step may be useful if a large data set needs to be segmented, making it reasonable to segment some images manually for error correction. The method could be trained on a small subset of the manual and automatically segmented data, in a first pass, and the error corrections learned could be useful to segment the rest of the dataset.

Deformable organisms provide an adaptable framework to perform segmentation. They can encode a high-level plan into deformable models, to help them work together to accomplish segmentation tasks. The different control layers may be adapted to fit any type of segmentation tasks.

References

1. Boesen, K., Rehm, K., Schaper, K., Stoltzner, S., Woods, R., Luders, E., Rottenberg, D.: Quantitative comparison of four brain extraction algorithms. NeuroImage 22(3), 1255–1261 (2004)
2. Desbrun, M., Meyer, M., Schroder, P., Barr, A.: Implicit fairing of irregular meshes using diffusion and curvature flow. In: Proceedings of the 26th Annual Conference on Computer Graphics and Interactive Techniques. pp. 317–324. ACM Press/Addison-Wesley Publishing Co. (1999)
3. Freund, Y., Schapire, R.: A desicion-theoretic generalization of on-line learning and an application to boosting. In: Computational Learning Theory. pp. 23–37. Springer (1995)

4. Gering, D., Nabavi, A., Kikinis, R., Hata, N., ODonnell, L., Grimson, W., Jolesz, F., Black, P., Wells III, W.: An integrated visualization system for surgical planning and guidance using image fusion and an open MR. Journal of Magnetic Resonance Imaging 13, 967–975 (2001)
5. Gharachorloo, N., Gupta, S., Sproull, R., Sutherland, I.: A characterization of ten rasterization techniques. ACM SIGGRAPH Computer Graphics 23(3), 355–368 (1989)
6. Hamarneh, G., McIntosh, C.: Physics-based deformable organisms for medical image analysis. In: Society of Photo-Optical Instrumentation Engineers (SPIE) Conference Series. vol. 5747, pp. 326–335 (2005)
7. Huttenlocher, D., Klanderman, G., Rucklidge, W.: Comparing images using the Hausdorff distance. IEEE Transactions on Pattern Analysis and Machine Intelligence pp. 850–863 (1993)
8. Ibanez, L., Schroeder, W., Ng, L., Cates, J., et al.: The ITK software guide. Kitware Inc (2005)
9. Jenkinson, M., Smith, S.: A global optimisation method for robust affine registration of brain images. Medical Image Analysis 5(2), 143–156 (2001)
10. Joshi, A., Lepore, N., Joshi, S., Lee, A., Barysheva, M., Stein, J., McMahon, K., Johnson, K., de Zubicaray, G., Martin, N., et al.: The contribution of genes to cortical thickness and volume. NeuroReport 22(3), 101 (2011)
11. Klein, A., Andersson, J., Ardekani, B., Ashburner, J., Avants, B., Chiang, M., Christensen, G., Collins, D., Gee, J., Hellier, P., et al.: Evaluation of 14 nonlinear deformation algorithms applied to human brain MRI registration. NeuroImage 46(3), 786–802 (2009)
12. Lorensen, W., Cline, H.: Marching cubes: A high resolution 3D surface construction algorithm. ACM Siggraph Computer Graphics 21(4), 163–169 (1987)
13. McInerney, T., Hamarneh, G., Shenton, M., Terzopoulos, D.: Deformable organisms for automatic medical image analysis. Medical Image Analysis 6(3), 251–266 (2002)
14. McInerney, T., Terzopoulos, D.: Deformable models in medical image analysis: a survey. Medical Image Analysis 1(2), 91–108 (1996)
15. McIntosh, C., Hamarneh, G.: I-DO: A Deformable Organisms framework for ITK. Medical Image Analysis (2006)
16. McIntosh, C., Hamarneh, G.: Spinal crawlers: Deformable organisms for spinal cord segmentation and analysis. Medical Image Computing and Computer-Assisted Intervention–MICCAI 2006 pp. 808–815 (2006)
17. McIntosh, C., Hamarneh, G.: Vessel crawlers: 3D physically-based deformable organisms for vasculature segmentation and analysis. In: Computer Vision and Pattern Recognition, 2006 IEEE Computer Society Conference on. vol. 1, pp. 1084–1091 (2006)
18. McIntosh, C., Hamarneh, G., Mori, G.: Human limb delineation and joint position recovery using localized boundary models. In: Motion and Video Computing, 2007. WMVC'07. IEEE Workshop on. pp. 31–31. IEEE (2007)
19. Ohtake, Y., Belyaev, A., Bogaevski, I.: Polyhedral surface smoothing with simultaneous mesh regularization. In: Geometric Modeling and Processing 2000. Theory and Applications. Proceedings. pp. 229–237. IEEE (2000)
20. Pineda, J.: A parallel algorithm for polygon rasterization. ACM SIGGRAPH Computer Graphics 22(4), 17–20 (1988)
21. Prasad, G., Joshi, A., Thompson, P., Toga, A., Terzopoulos, D., Shattuck, D.: Skull-stripping with deformable organisms. In: International Symposium on Biomedical Imaging, ISBI 2011. pp. 1662–1665. IEEE (2011)

22. Resnick, S., Pham, D., Kraut, M., Zonderman, A., Davatzikos, C.: Longitudinal magnetic resonance imaging studies of older adults: a shrinking brain. Journal of Neuroscience 23(8), 3295–3301 (2003)
23. Roche, A., Malandain, G., Pennec, X., Ayache, N.: The correlation ratio as a new similarity measure for multimodal image registration. Medical Image Computing and Computer-Assisted Interventation–MICCAI 1998 p. 1115 (1998)
24. Segonne, F., Dale, A., Busa, E., Glessner, M., Salat, D., Hahn, H., Fischl, B.: A hybrid approach to the skull stripping problem in MRI. NeuroImage 22(3), 1060–1075 (2004)
25. Shattuck, D., Leahy, R.: BrainSuite: an automated cortical surface identification tool. Medical Image Analysis 6(2), 129–142 (2002)
26. Shattuck, D., Mirza, M., Adisetiyo, V., Hojatkashani, C., Salamon, G., Narr, K., Poldrack, R., Bilder, R., Toga, A.: Construction of a 3D probabilistic atlas of human cortical structures. NeuroImage 39(3), 1064–1080 (2008)
27. Shattuck, D., Prasad, G., Mirza, M., Narr, K., Toga, A.: Online resource for validation of brain segmentation methods. NeuroImage 45(2), 431–439 (2009)
28. Smith, S.: Fast robust automated brain extraction. Human Brain Mapping 17(3), 143–155 (2002)
29. Steels, L.: The artificial life roots of artificial intelligence. Artificial Life 1(1_2), 75–110 (1993)
30. Terzopoulos, D., Platt, J., Barr, A., Fleischer, K.: Elastically deformable models. ACM Siggraph Computer Graphics 21(4), 205–214 (1987)
31. Thompson, P., Hayashi, K., De Zubicaray, G., Janke, A., Rose, S., Semple, J., Herman, D., Hong, M., Dittmer, S., Doddrell, D., et al.: Dynamics of gray matter loss in Alzheimer's disease. Journal of Neuroscience 23(3), 994–1005 (2003)
32. Thompson, P., Hayashi, K., Sowell, E., Gogtay, N., Giedd, J., Rapoport, J., De Zubicaray, G., Janke, A., Rose, S., Semple, J., et al.: Mapping cortical change in Alzheimer's disease, brain development, and schizophrenia. NeuroImage 23, S2–S18 (2004)
33. Wang, H., Das, S., Suh, J., Altinay, M., Pluta, J., Craige, C., Avants, B., Yushkevich, P.: A Learning-Based Wrapper Method to Correct Systematic Errors in Automatic Image Segmentation: Consistently Improved Performance in Hippocampus, Cortex and Brain Segmentation. NeuroImage (2011)
34. Woods, R., Dapretto, M., Sicotte, N., Toga, A., Mazziotta, J.: Creation and use of a Talairach-compatible atlas for accurate, automated, nonlinear intersubject registration, and analysis of functional imaging data. Human Brain Mapping 8(2-3), 73–79 (1999)